Journal of Chromatography A, 1217 (2010) 2032–2041

Contents lists available at ScienceDirect

Journal of Chromatography A

journal homepage: www.elsevier.com/locate/chroma

Modeling protein binding and elution over a chromatographic surface probed by surface plasmon resonance

Tiago Vicente[a,b], José P.B. Mota[c], Cristina Peixoto[a], Paula M. Alves[a,b], Manuel J.T. Carrondo[a,b,d,*]

[a] IBET, Apartado 12, P-2781-901 Oeiras, Portugal
[b] ITQB-UNL, 2780-157 Oeiras, Portugal
[c] Requimte/CQFB, Departamento de Química, FCT/UNL, P-2829-516 Caparica, Portugal
[d] FCT/UNL, P-2829-516 Caparica, Portugal

ARTICLE INFO

Article history:
Received 23 October 2009
Received in revised form
14 December 2009
Accepted 22 January 2010
Available online 1 February 2010

Keywords:
Surface plasmon resonance
Ion-exchange chromatography
Modeling

ABSTRACT

Surface plasmon resonance (SPR) spectroscopy is used as a scaled-down, analytical, pseudo-chromatography tool for analyzing protein binding and elution over an ion-exchange surface under cyclic sorption conditions. A micrometric-scale adsorption surface was produced by immobilizing a typical ion exchange ligand – diethylaminoethyl (DEAE) – onto commercially available planar gold sensor chip surfaces pre-derivatized with a self-assembled monolayer of 11-mercaptoundecanoic acid with known density. An explicit mathematical formulation is provided for the deconvolution and interpretation of the SPR sensorgrams. An adsorption rate model is proposed to describe the SPR sensorgrams for bovine serum albumin, used here as model protein, when the DEAE surface is subjected to a cyclic series of binding and elution steps. Overall, we demonstrate that the adsorption rate model is capable of quantitatively describing BSA binding and elution for protein titers from dilute conditions up to overloaded conditions and a broad range of salt concentrations.

1. Introduction

Process design and optimization are critical tasks in any pharmaceutical industrial process; the time and resources allotted for R&D tasks are relevant issues [1,2]. This becomes particularly crucial within the scope of biopharmaceuticals for gene therapy or vaccination, comprising complex structures, such as monoclonal antibodies, virus-like particles, or viruses. Indeed, these products commonly derive from highly costly animal cell-based upstream productions. Hence, the optimization of such processes becomes mandatory in the interest of cost and time savings. Scaled-down models, often used in high-throughput technologies, are being considered as viable options for early stage process development [3–5], including downstream processing steps such as ion-exchange chromatography, which is one of the core purification steps for biopharmaceuticals [6–13]. High-throughput robotics operating with multi-micro-sized matrices are able to generate a considerable amount of data covering the *n*-dimensional design space for the selected *n*-critical process variables [14]. By using these high-throughput methodologies, the bottleneck seems now to be moving towards data processing and subsequent integration. This drawback opens up the need for a more focused scaled-down rationale, capable of ultimately yielding better and more selective data for facilitating further optimization choices. In the context of multicomponent adsorption processes, including ion-exchange chromatography, the understanding of how the different contaminants interact with the stationary phase provides clues and guidelines for finding the best strategy for process design and optimization.

Surface plasmon resonance (SPR) is a spectroscopic technique with a wide variety of applications (established over the last couple of decades) whenever an interaction between two entities is involved— a ligand, immobilized on a surface, and an analyte, flowing over that surface [15–17]. Moreover, SPR permits simpler and faster label-free, real-time interaction analyzes between those two entities than other analytical technologies [18]. By producing interaction data using highly reduced amounts of material in each run, SPR can play a significant role in the design of adsorption processes, including ion-exchange chromatography. Such analytical technology may be used as a cost-effective aid for the early stage systematic screenings of stationary phases, buffer conditions, and chromatographic steps.

An SPR sensor mainly consists of a surface support with a metal (typically gold) and a film of fluid flowing over the surface, thus allowing for possible interactions between the gold surface and the liquid. Commercially available SPR-based sensors can be extremely sensitive; in fact, they can detect, within a fraction of a second,

* Corresponding author at: IBET/ITQB-UNL, Apartado 12, P-2781-901 Oeiras, Portugal. Tel.: +351 214469360; fax: +351 214421161.
E-mail addresses: mjtc@ibet.pt, mjtc@itqb.unl.pt (M.J.T. Carrondo).

0021-9673/$ – see front matter © 2010 Elsevier B.V. All rights reserved.
doi:10.1016/j.chroma.2010.01.068

very small refractive index (RI) changes within the film delimited in the depth of the sensing evanescent electromagnetic field [19]. When such a sensor is functionalized with selective ligands for any given molecule (either chemical or biochemical), then selective (bio)chemical sensors can be custom-made. A straightforward and self-controlled means to prepare a functionalized sensor surface from an untreated gold one is to use self-assembled monolayers (SAMs) using thiolate compounds [20]. SAMs – particularly those formed by adsorption of long chain alkanethiols over gold surfaces – are especially suited for studying interactions between post-functionalized surfaces and proteins or other particles [20]. These compounds self-generate well defined, synthetic surfaces with known molecular and macroscopic properties, thus allowing for consistent fundamental studies. This is particularly relevant if a SAM is used as a linker to a layer of covalently coupled functional groups (at known stoichiometry) [21]. 11-Mercaptoundecanoic acid (MUA) has been utilized in different applications for the covalent immobilization of ligands to study complex biological analytes, such as viruses [22,23].

The quantitative interpretation and modeling of SPR rendered data, including cases where different SAM layers are used, has been addressed in the literature [18,19]. However, a detailed analysis for a sensor chip surface functionalized with a layer of ion-exchange ligands, mimicking the undergoing mechanisms of adsorption equilibrium and kinetics on a typical adsorbent surface, is still unavailable.

In the present work SPR spectroscopy is used as a scaled-down, analytical tool for analyzing protein binding and elution over an ion-exchange surface under cyclic adsorption conditions. We review the principles of SPR spectroscopy and establish the required calibration procedures and analytical formulae for converting the SPR signal shift into surface concentration of adsorbed protein. We propose two different adsorption rate models that qualitatively describe the general trends observed in the SPR sensorgrams for bovine serum albumin (BSA) – used here as model protein – when the DEAE surface is subjected to a cyclic series of binding and elution steps. By carefully analyzing the adsorption/desorption plateaus we show that it is possible to exclude one of the kinetic models. Furthermore, by performing SPR experiments at different salt concentrations, the dependency of binding capacity and rate constants on salt concentration can be established. Overall, we demonstrate that the resulting adsorption rate model quantitatively describes the SPR sensorgrams for protein titers from dilute conditions up to overloaded conditions and a broad range of salt concentrations.

2. Materials and methods

2.1. Sensor surface preparation

Biacore gold sensor chip surfaces (Biacore/GE Healthcare, Uppsala, Sweden) were modified according to protocols described in the literature [20,22], but with some adjustments. 11-Mercaptoundecanoid acid (MUA) (NanoThinks™ ACID11 solution from Sigma–Aldrich, München, Germany) and 2-diethylaminoethylamine (DEAEA) (99% purity grade from Sigma–Aldrich) were used as thiolate for SAM preparation and ligand coupling compound, respectively. A Leica AR200 digital handheld refractometer (Leica Microsystems, Wetzlar, Germany) was used to monitor the RI changes throughout the MUA-SAM immobilization procedure.

The gold sensor chip surface was first equilibrated with ultrapure, deionized water, at 18.2 MΩ cm. The surface was sanitized with 0.1 M NaOH and 1% Triton™ X-100 (Sigma–Aldrich) and then re-equilibrated in 10 mM 4-morpholineethanesulfonic (MES) acid buffer (Sigma–Aldrich) at pH 5.0. Ethanol was then used to washout the buffer and the surface was exposed directly to the ACID11 solution (5 mM MUA in ethanol) and left overnight in a closed compartment inside a laminar flow bench. The freshly formed SAM of MUA was rinsed with ethanol and re-equilibrated with the 10 mM MES buffer previously used until the RI stabilized. The sensor chip was then docked into the SPR system – a Biacore™ 2000 (Biacore/GE Healthcare) – for DEAEA immobilization by amide coupling chemistry. The same MES solution was used as running buffer for the duration of the immobilization procedure.

Freshly prepared solutions of 0.4 M 1-ethyl-3-(3-dimethylamino-propyl)carbodiimide hydrochloride (EDC) and 1.0 M N-hydroxysuccinimide (NHS) (amine coupling kit from Biacore/GE Healthcare) in water were mixed 1:1 and injected in a pulse of 200 μL at 20 μL/min to activate the terminal carboxyl group for amide bond formation. 1.0 M DEAEA in MES running buffer was added in serial 100 μL pulses at 20 μL/min until the SPR signal stabilized. Although there are four flow sensing cells available in the Biacore sensor chip, only one flow cell was derivatized with DEAEA to allow the comparison of SPR adsorption data from MUA against MUA-DEAE. All buffers and solutions were prepared sterile and degassed prior to use.

2.2. SPR experiments

The SPR experiments were performed on a Biacore 2000 system at 25 °C. Analytical grade (> 98% electrophoresis purity) BSA was purchased from Merck KGaA (Darmstadt, Germany). It is well known that commercial BSA samples contain a substantial fraction (5–20%) of covalent dimmer; the actual amount in our freshly prepared BSA solutions is estimated to be ca. 6%, from analytical size-exclusion chromatography on a Superdex 200 column. This residual fraction is believed to have only a minor influence on the experimental results. This assumption is supported by the closeness between our estimate of the thickness of the adsorbed monolayer, obtained from calibration experiments at a high salt concentration (see discussion below), and the BSA diameter calculated from its molecular weight and mass density; these two lengths are much smaller than the diameter of the covalent dimmer. All buffers were prepared sterile and degassed prior to use in the equipment.

The experiments were performed at constant flow rate of running buffer and sample injection of 100 μL/min. Each run consisted of the following sequence of steps repeated over three or four cycles: (i) equilibration of the flow cell with running buffer at a prescribed NaCl concentration (c_0); (ii) injection of 100 μL of BSA solution at given concentration (c_0, c_B); (iii) desorption and equilibration with running buffer (again, at c_0). Before starting a new run, the flow cell was subjected to an aggressive desorption step using 100 μL of 1.5 M NaCl in 20 mM phosphate buffer at pH 6.8 ($c_{0,ref}$), and then cleaned/sanitized with 100 μL of 0.1 M NaOH for complete regeneration of the surface.

DEAE ligands and SAM's have been shown to be fully resistant to pulses of NaOH (or HCl) up to 1 M [24]. The baseline stability was controlled throughout the course of each experiment. All sensorgrams were duplicated by repeating each run once for confirmation of their reproducibility and surface regeneration.

3. Supporting theory for SPR data analysis

In order to quantitatively analyze SPR data under adsorption conditions one must first understand the underlying probing mechanism of the Biacore machine—the medium's RI within the sensing evanescent field depth. The RI of an aqueous salt solution (0) with concentration c_0 is

$$\eta_0 = \tilde{\eta}_w + (\tilde{\eta}_0 - \tilde{\eta}_w)\nu_0 c_0, \quad (1)$$

where c_0 (M) is the salt concentration, ν_0 is the molar volume of the salt ions (M^{-1}), $\tilde{\eta}_w$ is the RI of water, and $\tilde{\eta}_0$ is the RI of the salt ions. Similarly, the RI of the aqueous salt solution with a given dissolved solute (B) (this can take the form of any analyte, e.g., a protein), can be expressed as

$$\eta_B = \eta_0 + (\tilde{\eta}_B - \eta_0)\nu_B c_B, \tag{2}$$

where c_B (M), ν_B (M^{-1}) and $\tilde{\eta}_B$ are the concentration, specific volume, and RI of the dissolved solute, respectively.

The Biacore's signal, $R(\eta)$, expressed in resonance units (RU), is a function of the measured RI in the flow cell, η; if η does not vary greatly (i.e., if the shift $\Delta\eta$ is not very large), then the corresponding change in the Biacore signal, ΔR, will be proportional to the change in η, that is, $\Delta R = m\,\Delta\eta$ [19]. It is also known that η is not probed uniformly over the depth of the flow cell height, but proportionally to the intensity of light at each point. Thus, the effective RI measured by the Biacore system, η_{eff}, is the average of η over the depth of the evanescent electromagnetic field [19]:

$$\eta_{eff} = \frac{1}{d_p}\int_0^\infty \eta(z)e^{-z/d_p}\,dz, \tag{3}$$

where d_p is the effective penetration depth; for the case of the Biacore 2000 machine, $d_p \approx 150$ nm.

Let us first consider the case of a uniform adsorbent film of thickness d_s, attached to the metal sensor surface, under conditions where there is no adsorption from the fluid solution flowing over its surface (this is the case, e.g., when the salt concentration is large enough to suppress solute binding). The RI of this adsorbent film, η_s, is constant unless there are external perturbations, such as a temperature change in the flow cell, which is not the case in the present work. Assuming that η_s is constant, Eq. (3) can be rewritten as follows:

$$\begin{aligned}\eta_{eff} &= \frac{\eta_s}{d_p}\int_0^{d_s} e^{-z/d_p}\,dz + \frac{1}{d_p}\int_{d_s}^\infty \eta(z)e^{-z/d_p}\,dz\\ &= \eta_s(1-e^{-d_s/d_p}) + \frac{1}{d_p}\int_{d_s}^\infty \eta(z)e^{-z/d_p}\,dz\\ &= \eta_s(1-\phi_s) + \eta'_{eff},\end{aligned} \tag{4}$$

where $\phi_s = \exp(-d_s/d_p)$. In the absence of adsorption, $\eta(z) = \eta$ for $z > d_s$, where η is the bulk solution's RI, and $\eta'_{eff} = \eta\phi_s$. Therefore, under non-adsorbing conditions, η_{eff} is given by

$$\eta_{eff} = \eta_s + \phi_s(\eta - \eta_s). \tag{5}$$

When the salt solution has no dissolved solute ($c_0 > 0$, $c_B = 0$), the effective RI, $\eta_{0,eff}$, is given by Eq. (5) with η replaced by η_0 defined by Eq. (1); the result is

$$\eta_{0,eff} = \eta_s + \phi_s[(\tilde{\eta}_0 - \tilde{\eta}_w)\nu_0 c_0 + \tilde{\eta}_w - \eta_s]. \tag{6}$$

If the baseline (or reference) signal is established for a salt solution with concentration $c_{0,ref}$, then the change in the effective RI when the salt concentration is altered to c_0 is

$$(\eta_0 - \eta_{0,ref})_{eff} = \phi_s(\tilde{\eta}_0 - \tilde{\eta}_w)\nu_0(c_0 - c_{0,ref}). \tag{7}$$

The corresponding signal shift in the Biacore system is

$$\Delta R = m(\eta_0 - \eta_{0,ref})_{eff} = m_0(c_0 - c_{0,ref}), \tag{8}$$

where $m_0 = m\phi_s(\tilde{\eta}_0 - \tilde{\eta}_w)\nu_0$ is the slope of the linear fitting (with intercept set to zero) of ΔR against $(c_0 - c_{0,ref})$.

When solute is added to the reference salt solution ($c_0 = c_{0,ref}$, $c_B > 0$) and flown over the sensing surface under non-adsorbing conditions, the effective RI is given by

$$(\eta_{B,ref})_{eff} = \eta_s + \phi_s(\eta_{B,ref} - \eta_s), \tag{9}$$

where $\eta_{B,ref}$ is defined by Eq. (2) with $\eta_0 = \eta_{0,ref}$. The corresponding change in the RI is obtained as follows:

$$\begin{aligned}(\eta_{B,ref} - \eta_{0,ref})_{eff} &= \phi_s(\tilde{\eta}_B - \eta_{0,ref})\nu_B c_B\\ &= \phi_s[(\tilde{\eta}_B - \tilde{\eta}_w) - (\tilde{\eta}_0 - \tilde{\eta}_w)\nu_0 c_{0,ref}]\nu_B c_B\end{aligned} \tag{10}$$

and the shift of the Biacore signal is given by

$$\Delta R = m(\eta_{B,ref} - \eta_{0,ref})_{eff} = (m_B - m_0\nu_B c_{0,ref})c_B \tag{11}$$

where $m_B = m\phi_s(\tilde{\eta}_B - \tilde{\eta}_w)\nu_B$. Note that $m_B - m_0\nu_B c_{0,ref}$ is the slope of a linear fitting (with intercept set to zero) of ΔR vs c_B. Once m_0 and m_B are known, we can predict the shift in the Biacore signal due to the change in the effective RI, $(\eta_B - \eta_{0,ref})_{eff}$, of an aqueous buffer with salt concentration c_0 and solute concentration c_B (assuming that the baseline was defined for the buffer salt solution with concentration $c_{0,ref}$) using the expression:

$$\Delta R = (m_B - m_0 c_0\nu_B)c_B + m_0(c_0 - c_{0,ref}). \tag{12}$$

The more complex case where there is solute adsorption onto the adsorbent sensor surface film is depicted in Fig. 1. The aqueous buffer solution in the bulk has salt concentration c_0 and protein concentration c_B; the thickness of the adsorbed layer is d_m and its inter-solute volume is filled with buffer solution assumed to contain the same salt concentration as that of the bulk. In Fig. 1, d_m is assumed to be equal to the diameter of the adsorbed solute molecules, in accordance with the formulation of a single adsorbed monolayer, though this is not a restriction imposed in our formulation. The effective RI probed by the Biacore machine, $\eta_{m,eff}$, is

$$\begin{aligned}\eta_{m,eff} = \frac{\eta_s}{d_p}\int_0^{d_s} e^{-z/d_p}\,dz + \frac{\eta_m}{d_p}\int_{d_s}^{d_s+d_m} e^{-z/d_p}\,dz\\ + \frac{\eta_B}{d_p}\int_{d_s+d_m}^\infty e^{-z/d_p}\,dz,\end{aligned} \tag{13}$$

yielding

$$\eta_{m,eff} = \eta_s + \phi_s(\eta_m - \eta_s) + \phi_s\phi_m(\eta_B - \eta_m), \tag{14}$$

where $\phi_m = \exp(-d_m/d_p)$. Here, η_m and η_B are the RI's of the adsorbed monolayer and of the bulk aqueous solution (c_0, c_B), respectively.

Considering the adsorption model shown in Fig. 1, and assuming that the solute, when adsorbed, does not change neither its RI nor its specific (or molar) volume, then the adsorbed monolayer's RI is

$$\eta_m = \eta_0 + (\tilde{\eta}_B - \eta_0)\nu_B c_m, \tag{15}$$

where c_m (M) is the solute concentration in the volume occupied by the adsorbed monolayer; c_m can be converted into a surface concentration, q (g/dm^2), through the simple formula $q = d_m c_m$. If the

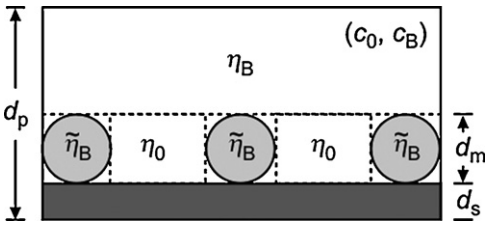

Fig. 1. Schematic of solute monolayer adsorbed onto the film of thickness d_s in the Biacore sensor chip flow cell. The bulk aqueous concentration has salt concentration c_0 and solute concentration c_B; the isolated (dry) solute's RI is $\tilde{\eta}_B$; aqueous solution is assumed to fill the gaps between adsorbed solute molecules, with salt concentration c_0 and RI η_0; the thickness of the adsorbed monolayer, d_m, is roughly equal to the diameter of the adsorbed solute.

baseline's RI is $(\eta_{0,\mathrm{ref}})_{\mathrm{eff}}$ (obtained with a salt solution of concentration $c_{0,\mathrm{ref}}$), then the change in the effective RI probed by the Biacore machine will be

$$(\eta_{\mathrm{m}} - \eta_{0,\mathrm{ref}})_{\mathrm{eff}} = \phi_{\mathrm{s}}(\eta_{\mathrm{m}} - \eta_{0,\mathrm{ref}}) + \phi_{\mathrm{s}}\phi_{\mathrm{m}}(\eta_{\mathrm{B}} - \eta_{\mathrm{m}}). \quad (16)$$

Expanding the two right-hand side differences yields:

$$(\eta_{\mathrm{m}} - \eta_{0,\mathrm{ref}})_{\mathrm{eff}} = \phi_{\mathrm{s}}(\tilde{\eta}_{\mathrm{B}} - \eta_0)\nu_{\mathrm{B}}[c_{\mathrm{m}} + \phi_{\mathrm{m}}(c_{\mathrm{B}} - c_{\mathrm{m}})] + \phi_{\mathrm{s}}(\eta_0 - \eta_{0,\mathrm{ref}}). \quad (17)$$

The corresponding shift in the Biacore signal is

$$\Delta R = (m_{\mathrm{B}} - m_0 c_0 \nu_{\mathrm{B}})[c_{\mathrm{m}} + \phi_{\mathrm{m}}(c_{\mathrm{B}} - c_{\mathrm{m}})] + m_0(c_0 - c_{0,\mathrm{ref}}). \quad (18)$$

Solving for c_{m} gives:

$$c_{\mathrm{m}} = \frac{\Delta R - m_0(c_0 - c_{0,\mathrm{ref}})}{(1-\phi_{\mathrm{m}})(m_{\mathrm{B}} - m_0 c_0 \nu_{\mathrm{B}})} - \frac{\phi_{\mathrm{m}}}{1-\phi_{\mathrm{m}}} c_{\mathrm{B}}. \quad (19)$$

Eqs. (18) and (19) are the most general ones since they encompass all the cases discussed above. For example, setting $\phi_{\mathrm{m}} = 1$ (i.e., $d_{\mathrm{m}} = 0$) eliminates the adsorbed monolayer; setting $c_{\mathrm{m}} = c_{\mathrm{B}}$ sets the solute concentration in the adsorbed monolayer equal to that in the bulk solution and the two phases become optically indistinguishable. In both cases, Eq. (18) correctly reduces to Eq. (12).

Eq. (11) shows that m_{B} can be determined from the slope b of the linear fitting (with intercept equal to zero) of ΔR against c_{B}, as $m_{\mathrm{B}} = b + m_0 \nu_{\mathrm{B}} c_{0,\mathrm{ref}}$. These calibration experiments, however, must be carried out under conditions where the solute does not adsorb; this may be difficult to achieve in practice. When the buffer conditions are such that a large fraction of the surface is shielded against adsorption, the adsorbed phase will quickly reach saturation conditions, that is, c_{m} will attain a constant value for moderate values of c_{B}. Eq. (18) shows that, in this case, a plot of ΔR against c_{B} still exhibits a linear relationship for sufficiently large values of c_{B} (i.e., those values of c_{B} for which $c_{\mathrm{m}} \approx$ const.), but with slope equal to $\phi_{\mathrm{m}}(m_{\mathrm{B}} - m_0 \nu_{\mathrm{B}} c_{0,\mathrm{ref}})$ and intercept equal to $(1-\phi_{\mathrm{m}})(m_{\mathrm{B}} - m_0 \nu_{\mathrm{B}} c_{0,\mathrm{ref}})c_{\mathrm{m}}$. Under these conditions, an estimate of ϕ_{m}, and of the resulting d_{m}, can be obtained by noticing that the slope of $(\eta_0 - \eta_{0,\mathrm{ref}})_{\mathrm{eff}}$ against $(c_0 - c_{0,\mathrm{ref}})$ yields $\phi_{\mathrm{s}}(\tilde{\eta}_0 - \tilde{\eta}_{\mathrm{w}})\nu_0 = m_0/m$ (cf. Eqs. (7) and (8)) and that the slope of $(\eta_{\mathrm{B}} - \eta_{0,\mathrm{ref}})_{\mathrm{eff}}$ against c_{B} gives $\phi_{\mathrm{s}}(\tilde{\eta}_{\mathrm{B}} - \eta_{0,\mathrm{ref}})\nu_{\mathrm{B}} = [\phi_{\mathrm{m}}(m_{\mathrm{B}} - m_0 \nu_{\mathrm{B}} c_{0,\mathrm{ref}})]/m$ (cf. Eqs. (10) and (11)); such measurements can be performed with a refractometer.

4. Adsorption/desorption rate model

In this section we formulate a general adsorption/desorption rate model capable of quantitatively explaining the SPR sensorgrams for the interaction of BSA with the DEAE-SAM surface under continuous cycling of the solute concentration. As described in Section 2.2, each SPR experiment consisted of a series of adsorption/desorption cycles, where during the adsorption step the sensor chip was contacted with buffer solution with given salt and protein concentrations; after binding, buffer alone was introduced to monitor the desorption kinetics. This sequence was repeated over three or four cycles. We observed partial irreversible binding of the protein onto the DEAE-SAM surface (or subject to a very slow dissociation kinetics which was imperceptible for the duration of the desorption step) and a slight increase of the binding plateau from cycle to cycle, but tending to a constant, asymptotical value.

Based on these observations, it is assumed that only part of the protein is reversibly adsorbed, whereas the other part binds irreversibly to the stationary phase. Moreover, we consider that the irreversible adsorption process is the result of two binding mechanisms operating in parallel: one in which irreversible adsorption takes place from the reversibly adsorbed phase, and another in which irreversible adsorption takes place directly from the liquid phase. Two possible types of irreversible binding mechanisms are considered: in mechanism A, irreversible adsorption from the reversibly adsorbed phase is an autonomous process that is independent of the protein concentration in the liquid phase; in mechanism B, irreversible adsorption from the reversibly adsorbed phase depends on the frequency of collisions or interactions between the proteins in the reversibly adsorbed phase and those contacting liquid solution. The two mechanisms are illustrated in Fig. 2.

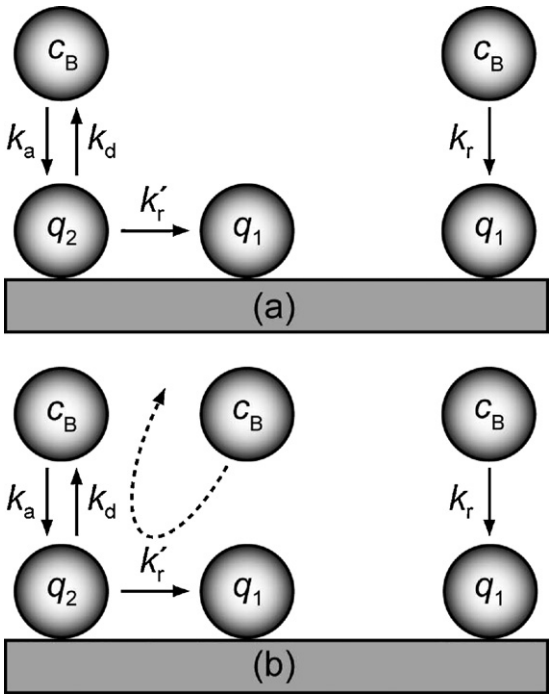

Fig. 2. Kinetic model for reversible/irreversible protein adsorption.

Let q_1 be the concentration of irreversibly bound protein and q_2 the protein concentration in the reversibly adsorbed phase. For mechanism A, the irreversible binding kinetics can be written as

$$\frac{dq_1}{dt} = k_{\mathrm{r}} c_{\mathrm{B}}(\tilde{q}_1^{\infty} - q_1) + k_{\mathrm{r}}' q_2, \quad (20)$$

where k_{r} is the rate constant for irreversible adsorption from the bulk, k_{r}' is the rate constant for irreversible binding from the reversibly adsorbed phase and $\tilde{q}_1^{\infty}$ is the apparent capacity of the stationary phase for irreversible binding; this capacity is apparent because some of the sites for irreversible binding may be shielded by the presence of reversibly adsorbed proteins. Hence

$$\tilde{q}_1^{\infty} = q_1^{\infty} - \sigma_{12} q_2, \quad (21)$$

where σ_{12} is a steric factor: it gives the number of irreversible binding sites shielded by the reversibly adsorbed proteins. For mechanism B, the corresponding equation is

$$\frac{dq_1}{dt} = k_{\mathrm{r}} c_{\mathrm{B}}(\tilde{q}_1^{\infty} - q_1) + k_{\mathrm{r}}' c_{\mathrm{B}} q_2. \quad (22)$$

The difference between mechanisms A and B is that for the former the rate of irreversible adsorption from the reversibly adsorbed phase is proportional to q_2 whereas for the latter it is proportional to $c_{\mathrm{B}} q_2$ (cf. Fig. 2).

Assuming a Langmuirian kinetic model for reversible adsorption, we can write for mechanism A:

$$\frac{dq_2}{dt} = k_{\mathrm{a}} c_{\mathrm{B}}(\tilde{q}_2^{\infty} - q_2) - (k_{\mathrm{d}} + k_{\mathrm{r}}')q_2, \quad (23)$$

where k_a and k_d are the forward and reverse rate constants for reversible adsorption, respectively, and $\tilde{q}_2^\infty$ is the apparent capacity of the stationary phase for reversible binding. Again, the adsorption capacity is apparent because some of the sites for reversible binding may be shielded by the presence of irreversibly adsorbed proteins:

$$\tilde{q}_2^\infty = q_2^\infty - \sigma_{21} q_1. \tag{24}$$

For mechanism B the kinetic model is

$$\frac{dq_2}{dt} = k_a c_B(\tilde{q}_2^\infty - q_2) - k_d q_2 - k_r' c_B q_2 = k_a c_B(\tilde{q}_2^\infty - q_2) - (k_d + k_r' c_B) q_2. \tag{25}$$

At equilibrium (which we denote by an overbar):

$$\left(\overline{\frac{dq_1}{dt}}\right) = \left(\overline{\frac{dq_2}{dt}}\right) = 0, \tag{26}$$

which allows us to determine closed-form expressions for the adsorption isotherms, $\bar{q}_1(c_B)$ and $\bar{q}_2(c_B)$.

One way to discriminate between the two types of irreversible binding mechanisms is to compare the dependencies between $\bar{q}_1$ and $\bar{q}_2$ given by Eqs. (20) and (22). For mechanism A, we get

$$\bar{q}_1 = q_1^\infty + \left(\frac{k_r'}{k_r} - \sigma_{12} c_B\right) \frac{\bar{q}_2}{c_B}, \tag{27}$$

whereas for mechanism B the expression is

$$\bar{q}_1 = q_1^\infty + \left(\frac{k_r'}{k_r} - \sigma_{12}\right) \bar{q}_2. \tag{28}$$

Clearly, for mechanism B, $\bar{q}_1$ varies linearly with $\bar{q}_2$ with an ordinate and a slope that are independent of c_B.

Let us assume temporarily that the shielding effect can be neglected. In this case, Eqs. (27) and (28) simplify to

$$\bar{q}_1 = q_1^\infty + \left(\frac{k_r'}{k_r}\right) \frac{\bar{q}_2}{c_B} \quad \text{(mechanism A)} \tag{29}$$

$$\bar{q}_1 = q_1^\infty + \left(\frac{k_r'}{k_r}\right) \bar{q}_2 \quad \text{(mechanism B)}. \tag{30}$$

Thus for mechanism A, $\bar{q}_1$ varies linearly with $\bar{q}_2/c_B$, whereas for mechanism B, $\bar{q}_1$ varies linearly with $\bar{q}_2$; in both cases the ordinate and slope are positive.

The saturation capacities, q_1^∞ and q_2^∞, and hence the total saturation capacity $q^\infty = q_1^\infty + q_2^\infty$, are expected to be modulated by the salt concentration, as is the case for a typical ion-exchange matrix. The higher the counterion concentration, the lower the binding of a given solute assuming that no other effects are impacting the overall adsorption process onto the SPR sensor chip. Thus, an empirical correlation of the form:

$$q^\infty = q_0^\infty e^{k c_0} \quad \text{or} \quad q^\infty = q_0^\infty c_0^k \tag{31}$$

is adopted here; in Eq. (31), q_0^∞ is the maximum attainable adsorption capacity at residual ionic strength and $k < -1$ is an empirical constant. The second expression for q^∞ in Eq. (31) is similar to the mathematical formulation used in the steric mass action formalism for the interpretation of adsorption by ion exchange [25].

5. Results and discussion

5.1. Calibration of Biacore signal

The Biacore signal was calibrated using various solutions with different salt (c_0) and BSA (c_B) concentrations and a baseline defined for a buffer solution with salt concentration $c_{0,ref} = 1.5$ M NaCl. First, salt solutions with different c_0 values were injected into the Biacore cell and the corresponding signal shifts measured (Fig. 3a). The linear fitting (with intercept set to zero) of ΔR against

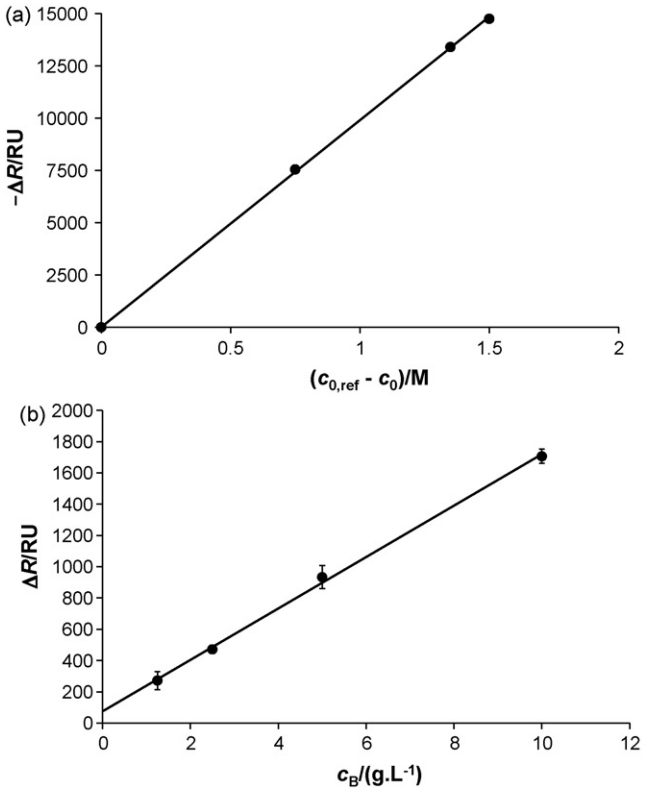

Fig. 3. (a) Experimental SPR signal shift, ΔR, as a function of salt concentration, $c_0 - c_{0,ref}$ ($c_{0,ref} = 1.5$ M NaCl) and (b) experimental SPR signal shift, ΔR, as a function of bulk protein concentration, c_B, under low binding conditions ($c_0 = c_{0,ref} = 1.5$ M NaCl).

($c_0 - c_{0,ref}$) yielded $m_0 = m\phi_s(\tilde{\eta}_0 - \tilde{\eta}_w)\nu_0 = 9898.1$ RU/M with an excellent regression coefficient ($r^2 = 0.9998$); this linearity is in complete agreement with Eq. (8). This calibration accounts for the salt concentration effect without the presence of solute in suspension.

To account for the effect of BSA in solution (c_0, $c_B > 0$) a set of BSA concentrations in buffer with salt concentration $c_0 = c_{0,ref} = 1.5$ M NaCl was used (Fig. 3b). This salt concentration was high enough to reduce BSA adsorption to a residual level, so that the Biacore signal shifts yielded a straight line when plotted against c_B in accordance with Eq. (18) when c_m has a constant value. The linear fitting of ΔR vs c_B yielded a slope $\phi_m(m_B - m_0\nu_B c_{0,ref}) = 164.43$ RU/(g/L), again with a very good regression coefficient: $r^2 = 0.9986$ (Fig. 3b).

The main physical properties of BSA are listed in Table 1[26]; from the data, $\nu_B = 7.553 \times 10^{-4}$ L/g, hence $m_0\nu_B c_{0,ref} = 10.92$ RU/(g/L) and $m_B = 164.43/\phi_m + 10.92 = 179.79$ RU/(g/L). Eq. (19) can now be applied for converting the SPR signal (ΔR) into concentration values of adsorbed protein, c_m (g/L) and $q(\text{g/dm}^2) = 10^{-8} d_m c_m$, with d_m in nm.

In solution, BSA is a prolate ellipse (cigar-shaped) with an axial ratio of about four; if the assumed BSA radius is calculated from its molecular weight and mass density, then the thickness of the planar monolayer will be $d_m = 2 \times 26.9$ Å $= 53.8$ Å [26]. According to our

Table 1
BSA physical properties [26].

Molecular weight	66.7 kDa
Dimensions	4 nm × 4 nm × 14 nm
Radius based on sphere	2.69 nm
Density	1360 g/L
Isoelectric point	4.9

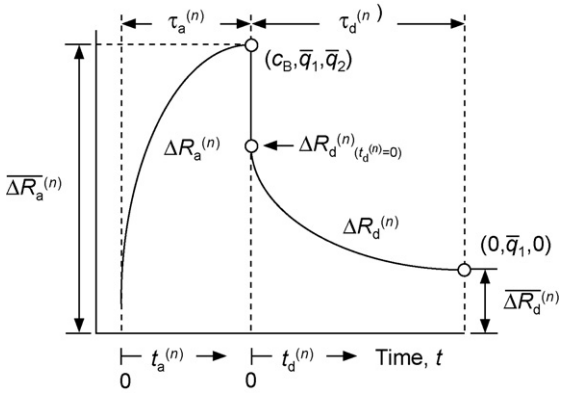

Fig. 4. Schematic of the n th adsorption/desorption cycle for a Biacore experiment.

model, d_m can be determined from the obtained values of m_0 and m_B and RI measurements as follows: plotting $(\eta_0 - \eta_{0,ref})_{eff}$ against $(c_0 - c_{0,ref})$ yields the slope:

$$\phi_s(\tilde{\eta}_0 - \tilde{\eta}_w)\nu_0 = \frac{m_0}{m} \tag{32}$$

and plotting $(\eta_B - \eta_{0,ref})_{eff}$ against c_B yields the slope:

$$\phi_s(\tilde{\eta}_B - \eta_{0,ref})\nu_B = \frac{\left[\phi_m(m_B - m_0\nu_B c_{0,ref})\right]}{m}. \tag{33}$$

From these linear plots the calculated value d_m is $d_{m,\eta\text{-based}} \approx 5.6$ nm, which is closely comparable to the reference value of 5.38 nm. This supports the applicability of Eqs. (18) and (19) derived from our theory for SPR data analysis.

5.2. Analysis of BSA sensorgrams

The SPR experiments were performed at Biacore's maximum flow rate (100 μL/min) to avoid mass transfer limitations. These were, in fact, negligible when compared to the sorption rates at the tested conditions; a two-compartment, mass transport model coupled to our kinetic model showed no detectable impact on the apparent adsorption/desorption rates (see Appendix A).

Fig. 4 shows the schematic of an adsorption/desorption cycle (say the nth one) for a Biacore experiment. The durations of the adsorption and desorption steps are $\tau_a^{(n)}$ and $\tau_d^{(n)}$, respectively. At the end of the adsorption step the SPR signal is $\overline{\Delta R}_a^{(n)}$ and corresponds to $\{c_B, \bar{q}_1^{(n)}, \bar{q}_2^{(n)}\}$, i.e., {bulk protein} + {irreversibly adsorbed protein} + {reversibly adsorbed protein}. When the desorption step begins, the bulk protein is immediately removed due to the high flow rate used (100 μL/min) compared to the flow chamber volume (approximately 60 nL) and the conditions in the flow cell change to $\{0, \bar{q}_1^{(n)}, \bar{q}_2^{(n)}\}$; the SPR signal then decays until it stabilizes at a value $\overline{\Delta R}_d^{(n)}$ corresponding to $\{0, \bar{q}_1^{(n)}, 0\}$, i.e., when only irreversibly adsorbed protein remains in the sensor chamber.

If the step durations, $\tau_a^{(n)}$ and $\tau_d^{(n)}$, are long enough, then the SPR signals, $\overline{\Delta R}_a^{(n)}$ and $\overline{\Delta R}_d^{(n)}$, at the end of the respective steps correspond to steady state conditions in the sensor chamber (which are denoted by an overbar in our rate model); these are characterized by an horizontal plateau in the sensorgrams (i.e., the SPR signal becomes constant). This was found to be the case for most of the runs, particularly for the desorption steps. For those cases where the SPR signal had not yet attained a constant value at the end of the step, the signal was extrapolated to infinite time by fitting the asymptotic part of the signal to a first-order dynamics:

$$\Delta R(t) = \alpha - \beta \exp(-t/\tau), \tag{34}$$

where α, β and $\tau > 0$ are fitting parameters; the asymptotic value of $\Delta R(t)$ for large values of time was estimated as the value of the fitted parameter α. Using Eq. (18), the value of $\overline{\Delta R}_a^{(n)}$ was converted into the value of $\bar{q}_1^{(n)} + \bar{q}_2^{(n)}$ and that of $\overline{\Delta R}_d^{(n)}$ into the value of $\bar{q}_1^{(n)}$.

From the analysis of the adsorption/desorption plateaus it is possible to make a first assessment of the adequacy of the two rate models – mechanisms A and B developed in Section 4 – incorporating different mechanisms for irreversible binding. According to mechanism A, $\bar{q}_1^{(n)}$ should vary linearly with $\bar{q}_2^{(n)}/c_B$ with positive ordinate and slope, whereas for mechanism B, $\bar{q}_1^{(n)}$ should change linearly with $\bar{q}_2^{(n)}$ with positive ordinate and slope. As shown in Fig. 5, the experimental results reject mechanism A and support mechanism B.

Therefore, the most suitable kinetic model (mechanism B) can be stated as

$$\frac{dq_1}{dt} = k_r c_B(q_1^\infty - \sigma_{12}q_2 - q_1) + k_r' c_B q_2, \tag{35}$$

$$\frac{dq_2}{dt} = k_a c_B(q_2^\infty - \sigma_{21}q_1 - q_2) - (k_d + k_r' c_B)q_2. \tag{36}$$

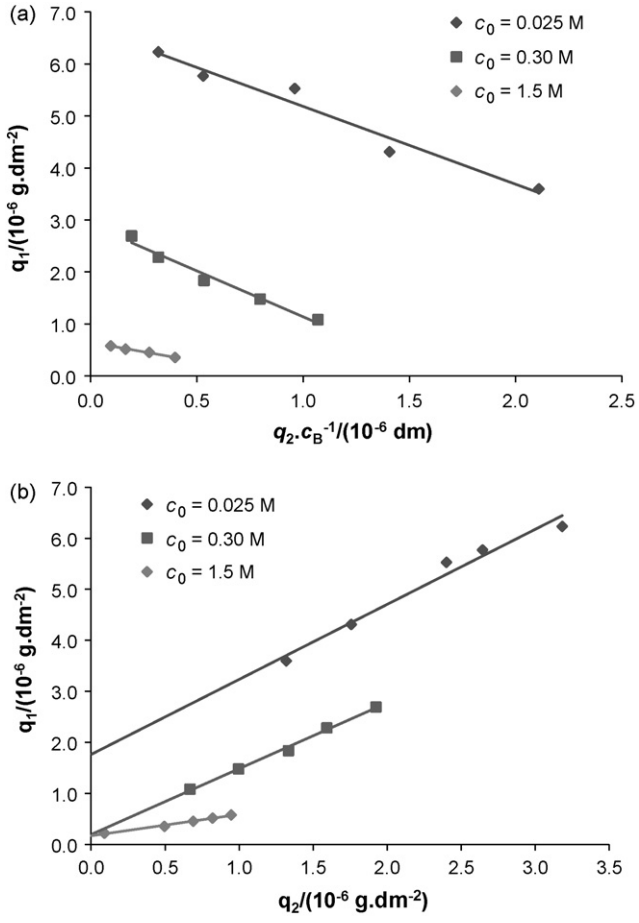

Fig. 5. Evaluation of the suitability of mechanisms A and B for the description of the dynamics of the SPR adsorption/desorption cycles: (a) $\bar{q}_1$ vs $\bar{q}_2/c_B$ plot (mechanism A); linear regression coefficient, r^2, is 0.964, 0.975, and 0.983 for $c_0 = 0.025$ M, $c_0 = 0.30$ M, and $c_0 = 1.5$ M, respectively; note that all slopes are negative in disagreement with Eq. (29); (b) $\bar{q}_1$ vs $\bar{q}_2$ plot (mechanism B); r^2 is 0.951, 0.995, and 0.999 for $c_0 = 0.025$ M, $c_0 = 0.30$ M, and $c_0 = 1.5$ M, respectively; note that all slopes are positive in agreement with Eq. (30).

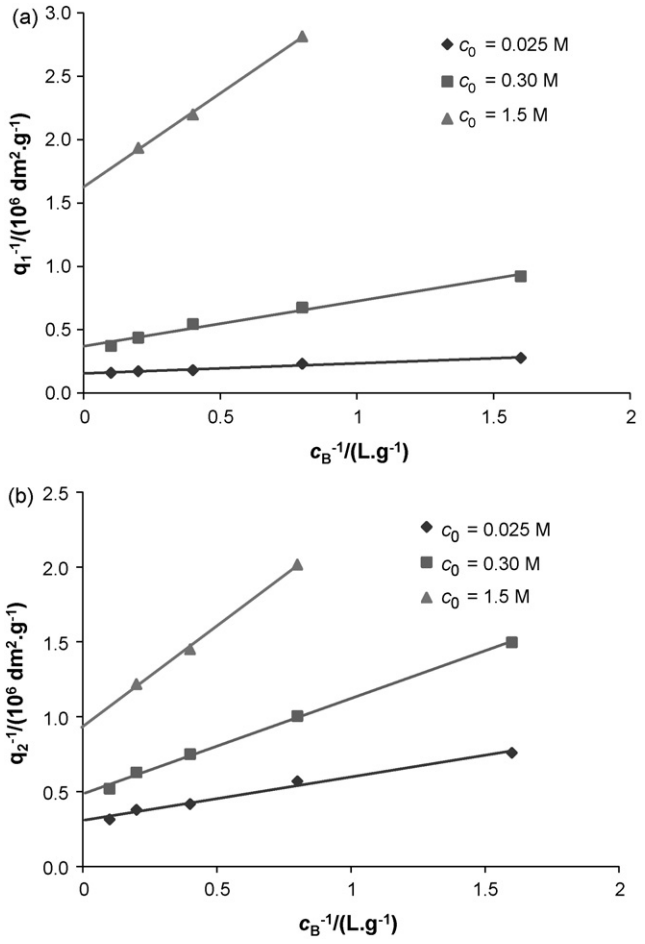

Fig. 6. Inverse plots of adsorption against bulk concentration: (a) $1/\bar{q}_1$ vs $1/c_B$; linear regression coefficient, r^2, is 0.999, 0.984, and 0.975 for $c_0 = 0.025$ M, $c_0 = 0.30$ M, and $c_0 = 1.5$ M, respectively; (b) $1/\bar{q}_2$ vs $1/c_B$; r^2 is 0.998, 0.998, and 0.986 for $c_0 = 0.025$ M, $c_0 = 0.30$ M, and $c_0 = 1.5$ M, respectively.

For this type of kinetic model, the reversible adsorption isotherm (i.e., the equilibrium dependency of $\bar{q}_2$ with c_B) is

$$\bar{q}_2 = \frac{(q_2^\infty - \sigma_{21} q_1^\infty) k_a c_B}{k_d + [k_r' + k_a + \sigma_{21}(k_r'/k_r - \sigma_{12}) k_a] c_B}, \tag{37}$$

which is a Langmuir-type isotherm, i.e.:

$$\bar{q}_2 = \frac{\gamma b_2 c_B}{1 + b_2 c_B}, \tag{38}$$

where

$$b_2 = \frac{k_r' + k_a[1 + \sigma_{21}(k_r'/k_r - \sigma_{12})]}{k_d}, \quad \gamma b_2 = \frac{k_a(q_2^\infty - \sigma_{21} q_1^\infty)}{k_d}. \tag{39}$$

Fig. 6 shows plots of $1/\bar{q}_1$ and $1/\bar{q}_2$ against $1/c_B$. From the plot of the inverse of $\bar{q}_2$ against the inverse of c_B it is evident that Eq. (37) does apply for the reversible adsorption isotherm, $\bar{q}_2(c_B)$, and that the irreversible component, $\bar{q}_1(c_B)$, is the sum of a Langmuir isotherm model and a constant – derived in our model as q_1^∞ – in accordance with Eqs. (30) and (37) (cf. Fig. 6). Note that the linear regression coefficients in Fig. 6b are very acceptable, confirming the Langmuir-type adsorption behavior implied by Eq. (38). The inverse plot for $\bar{q}_1$ shows also a very reasonable correlation; this can be explained by Eq. (28), which expresses the irreversible adsorption component as an irreversible adsorption capacity (q_1^∞) plus a Langmuir-type isotherm ($\bar{q}_2$) scaled by a constant ($k_r'/k_r - \sigma_{12}$).

As shown in both inverse plots of Fig. 6, the slope and intercept are functions of the salt concentration showing evidence of an ion exchange-type mechanism modulated by the concentration of the salt counterion, Cl^-. Although it is not apparent from the inverse plots, the adsorption equilibrium data extracted from the various SPR sensorgrams span protein concentrations from dilute conditions, where Henry's law prevails, up to overloaded conditions, where the adsorbed monolayer is near completed.

Let us now analyze the adsorption and desorption rates. During the desorption step, $c_B = 0$; the equations governing the dynamics for this step (under the assumption of negligible mass transfer resistance between the bulk and the sensor surface) are:

$$\frac{dq_1^{(n)}}{dt} = 0, \tag{40}$$

$$\frac{dq_2^{(n)}}{dt} = -k_d q_2^{(n)}. \tag{41}$$

The solution is simply

$$q_1^{(n)} = \bar{q}_1^{(n)}, \quad q_2^{(n)} = \bar{q}_2^{(n)} \exp\left(-k_d t_d^{(n)}\right). \tag{42}$$

Therefore:

$$\ln q_2^{(n)} = \ln \bar{q}_2^{(n)} - k_d t_d^{(n)}, \tag{43}$$

which shows that the rate constant k_d can be estimated from a $\ln q_2^{(n)}$-vs-$t_d^{(n)}$ regression plot.

From Eq. (18) it easy to deduce that

$$\Delta R_d^{(n)} = \frac{(m_B - m_0 c_0 \nu_B)(1 - \phi_m)\left[\bar{q}_1^{(n)} + q_2^{(n)}\right]}{d_m} + m_0(c_0 - c_{0,ref}). \tag{44}$$

The irreversible component, $q_1^{(n)} = \bar{q}_1^{(n)}$, is constant during the desorption step, but the reversible component, $q_2^{(n)}$, decreases from $\bar{q}_2^{(n)}$ to 0 as $t_d^{(n)}$ advances from 0 towards large time (∞). Let $\overline{\Delta R}_d^{(n)} = \lim_{t_d^{(n)} \to \infty} \Delta R_d^{(n)}$; then

$$\Delta R_d^{(n)} - \overline{\Delta R}_d^{(n)} = \frac{(m_B - m_0 c_0 \nu_B)(1 - \phi_m) q_2^{(n)}}{d_m} \tag{45}$$

and

$$\ln\left[\Delta R_d^{(n)} - \overline{\Delta R}_d^{(n)}\right] = \ln\left[\frac{(m_B - m_0 c_0 \nu_B)(1 - \phi_m)}{d_m}\right] + \ln q_2^{(n)}. \tag{46}$$

Therefore, $\ln[\Delta R_d^{(n)} - \overline{\Delta R}_d^{(n)}]$ and $\ln q_2^{(n)}$ both change with time at the same rate; in both cases the slope of the linear change with t is k_d.

Table 2
Model parameters estimated from three Biacore training experiments with BSA injections at $c_B = 2.5$ g/L and different salt concentrations, c_0.

c_0 (M)	k_d (s^{-1})	k_r (dm^3 g^{-1} s^{-1})	k_r' (dm^3 g^{-1} s^{-1})	k_a (dm^3 g^{-1} s^{-1})	$10^6 q_1^\infty$ (g dm^{-2})	$10^6 q_2^\infty$ (g dm^{-2})	σ_{12}	σ_{21}
0.025	0.051	0.017	0.0192	0.034	2.79	5.29	≈ 0	0.023
0.300	0.056	0.017	0.0221	0.020	0.20	4.45	≈ 0	0.025
1.500	0.128	0.016	0.0031	0.085	0.17	1.13	≈ 0	0.025

Let us assume the case when shielding is negligible, i.e. when σ_{12} and σ_{21} both tend to 0. In this case, Eqs. (35) and (36) simplify to

$$\frac{dq_1}{dt} = k_r c_B(q_1^\infty - q_1) + k'_r c_B q_2, \quad (47)$$

$$\frac{dq_2}{dt} = q_2^\infty k_a c_B - [k_d + (k_a + k'_r)c_B]q_2. \quad (48)$$

From Eq. (30) it is possible to determine q_1^∞ and k'_r/k_r. Rearranging Eq. (37) gives

$$\frac{1}{\bar{q}_2} = \frac{k_a + k'_r}{q_2^\infty k_a} + \frac{k_d}{q_2^\infty k_a}\frac{1}{c_B} = \alpha + \beta\frac{1}{c_B}. \quad (49)$$

From the linear fitting of $\bar{q}_2$ vs c_B we get $q_2^\infty k_a = k_d/\beta$ and $k_a + k'_r = k_d\alpha/\beta$. With this analysis, values of k_d, $q_2^\infty k_a$ and $k_a + k'_r$ can be estimated; these are the required lumped parameters to solve Eq. (48). As to Eq. (47), the values of q_1^∞ and the ratio k'_r/k_r are already known; by curve fitting, k_r and k'_r parameters can be estimated and all remaining unknown parameters can easily be calculated.

Once all parameters were estimated using the procedure described above, their values were refined by taking protein shielding into account. In this case the shielding factors, σ_{12} and σ_{21}, were determined by nonlinear curve-fitting using the complete kinetic model. These fittings were performed using gPROMS, a software package for the modeling and simulation of lumped and distributed-parameter process models with combined discrete and continuous characteristics [27]. The fittings were applied to sets of sensorgrams obtained at different salt concentrations. Table 2 summarizes the model parameters obtained using the procedure explained above: starting from an estimate of k_d using Eq. (46), the simplified model (Eqs. (48) and (47)) was used to determine k_r; all parameters were then introduced in the complete model formulation (Eqs. (35) and (36)) to refine the parameters and to estimate values for σ_{12} and σ_{21}.

Fig. 7 shows the comparison between simulations and experimental data at different salt concentrations. The results indicate a fairly good agreement between the experimental curves and our adsorption/desorption rate model with the estimated parameters (Table 2). The proposed assumption that two distinct adsorption mechanisms occur simultaneously, one being reversible and similar to an exchange reaction between the free protein and a certain number of bound ions, and another, with an extremely low desorption rate, formally defined as an irreversible mechanism, seems to suit well the experimental data.

Table 2 shows that the total BSA binding capacity of the derivatized surface, $q_1^\infty + q_2^\infty$, is ca. 0.81 mg/m^2 at 25 mM salt concentration; this value is less than the 5 mg/m^2 typically found for a protein monolayer. It is important to note, however, that the binding capacity is strongly dependent on the ligand density of the derivatized surface, and our guess is that the ligand density was low in our MUA-DEAE surfaces. This guess is supported, in part, by the low values of the binding constants, e.g., $b_2 = 1.04$ L/g at 25 mM NaCl, derived from the Langmuir adsorption isotherm model (cf. Eqs. (38) and (39)). Another indication of low ligand density are the small values of the shielding factors, σ_{12} and σ_{21}, obtained from the fitting of the kinetic model; small values of σ indicate that the bound BSA molecules are spread over the derivatized surface with a mean distance between neighboring molecules large enough for the shielding to have only a mild effect.

Figs. 5b, 6, and 7, as well as Table 2, show that both the reversible and irreversible adsorption mechanisms are sensitive functions of the salt concentration. A speculation for this effect on the irreversible adsorption component is that the degree of solvation of both the protein and the DEAE ligand sites, which is directly a function of salt concentration, inhibits the irreversible adsorption mechanism as it does for the reversible part. Indeed, when

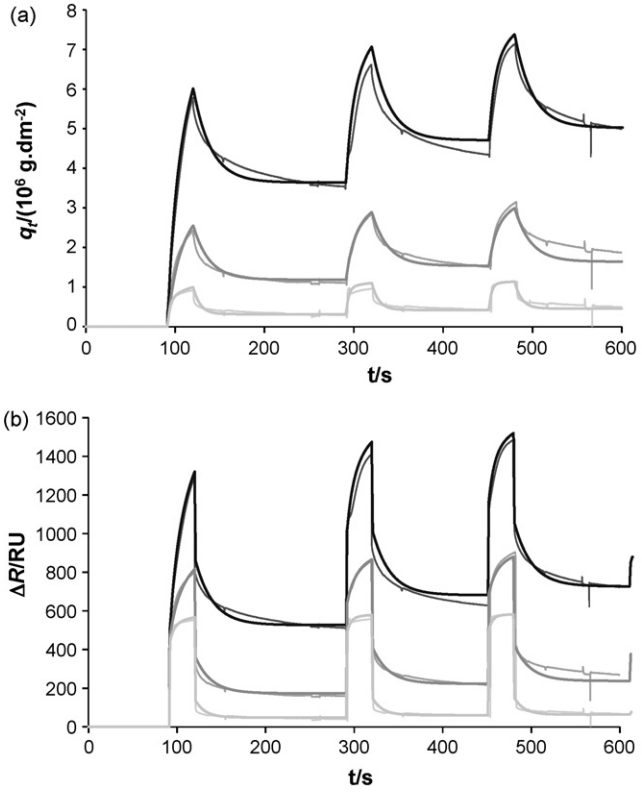

Fig. 7. Model training using three SPR experiments with BSA at $c_B = 2.5$ g/L and different salt concentrations, $c_0 = 0.025$, 0.30, and 1.5 M: (a) $q = q_1 + q_2$ vs t and (b) ΔR vs t. The thick and thin lines correspond, respectively, to the model predictions and experimental data; increasing dark tone in gray lines corresponds to decreasing salt concentrations; q is estimated from the experimental data using Eq. (19) and $d_m = 5.6$ nm.

the ionic strength or, more precisely, the salt concentration, are increased, both the reversible and irreversible equilibrium adsorption amounts decrease exponentially with the salt concentration, c_0. Thus, similar trends are observed for the dependencies of q_1^∞ and q_2^∞ with c_0: the larger the salt counterion concentration, the smaller the amount of adsorbed protein, in line with a typical ion-exchange surface using commercial matrices. These observations emphasize that the micrometric-scale DEAE surface mimics well an ion-exchange surface in terms of intrinsic adsorption capacities to different materials, even though other effects, such as the three-dimensionality of a chromatography matrix or mass transfer resistances, are not considered. Nevertheless, it is clear that by changing the ligand type and/or its density, which can be accomplished using different SAM compositions, our SPR-based method is well suited to small-scale studies of protein adsorption. In fact, a scale-down factor of over 1200-fold is accomplished using this strategy when compared to a commercially available Sartobind D MA 15 unit from Sartorius-Stedim Biotech (with 15 cm^2 total effective area).

In order to further validate the proposed model, SPR runs with different injected BSA concentrations were compared against predicted simulation curves; the results are shown in Fig. 8. This data set was used to test the extrapolation capability of the kinetic model with the parameter values estimated above. Note that the model parameters were estimated from SPR experiments at fixed c_B and varying c_0. The results depicted in Fig. 8 show that the changes in injected protein concentration are rather well predicted by the model simulations; additionally, changes in c_0 result in lower adsorption and faster kinetics confirming the expected low or residual adsorption.

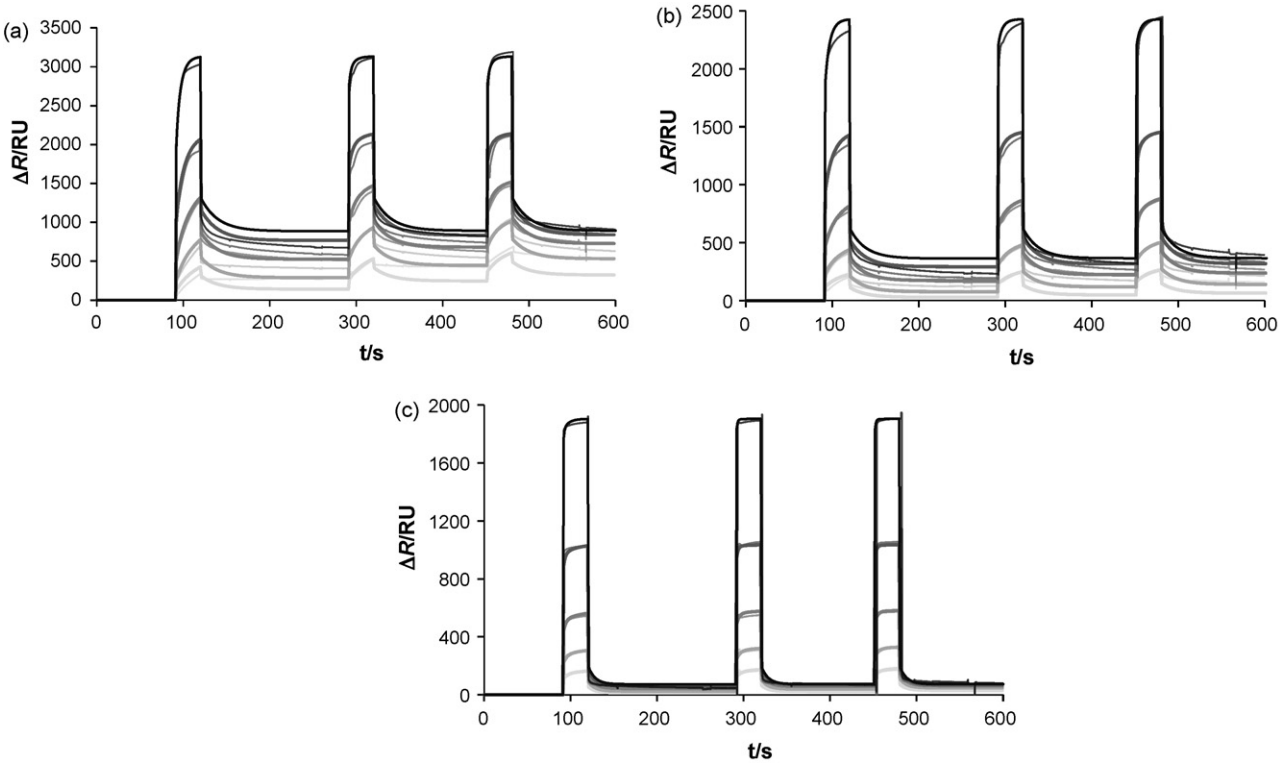

Fig. 8. Model validation with cyclic SPR experiments of BSA binding and elution over micrometric DEAE surface at different injected BSA concentrations, c_B = 0.625, 1.25, 2.5, 5, and 10 g/L; (a) c_0 = 0.025 M, (b) c_0 = 0.30 M, (c) c_0 = 1.5 M. The thick and thin lines correspond, respectively, to the model predictions and experimental data; increasing dark tone in gray lines corresponds to increasing protein concentration, c_B.

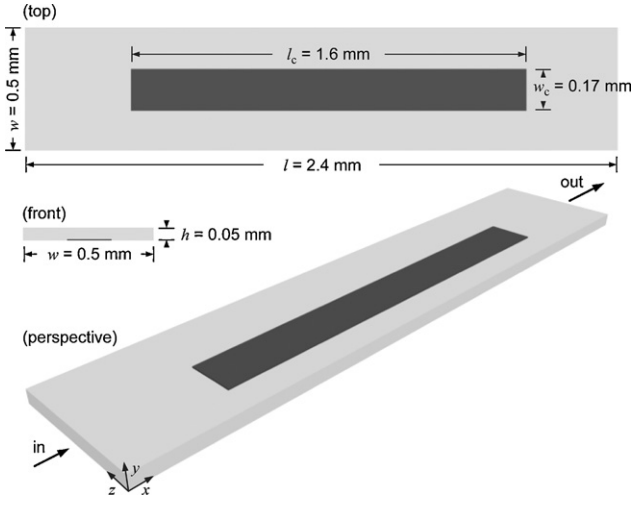

Fig. A.1. Schematic of Biacore's flow cell.

6. Conclusions

Adsorption equilibrium and kinetics on a derivatized surface, containing an ion-exchange functional DEAE group, have been measured and analyzed by SPR spectroscopy. BSA was used as a model protein for system development, implementation and testing. A complete mathematical description of the SPR sensor mechanism was derived giving rise to simple algebraic expressions relating the protein concentration in the adsorbed monolayer with SPR signal shift and protein and salt concentration in the bulk solution. Using the calibrations performed for salt and free protein in solution, the concentration of the adsorbed protein monolayer could be directly obtained from the SPR sensorgram data at different conditions of load and salt concentration.

An adsorption/desorption rate model, incorporating two different adsorption mechanisms, was proposed as a means to explain the SPR sensorgrams. The model is based on the assumption that only part of the protein adsorbs reversibly, according to a Langmuirian kinetic model, whereas the other part binds irreversibly to the DEAE surface; the kinetics of the latter is proportional to the protein concentrations in the bulk and in the reversibly adsorbed phase. The dependency between the estimated reversible and irreversible adsorbed concentrations in the stationary phase (herein mimicked by the customized chip surface) allowed us to discriminate between two possible adsorption mechanisms; this analysis suggests the presence of an adsorption scheme compatible with a first-order kinetics controlled by the reversibly adsorbed solute and its concentration in the mobile phase. From the SPR experiments it was possible to determine the adsorption isotherms for different salt conditions and to estimate the parameters of the developed rate model. The results provided evidence that the DEAE-SAM derivatized surface is a good mimic of an ion-exchange surface, as far as intrinsic ion exchange-related interactions are concerned, without considering transport or exclusion phenomena only present in a chromatographic matrix.

Acknowledgements

We acknowledge funding from the European Commission (Baculogenes, LSHB-2006-037541 and Clinigene – Network of Excellence, LSHB-2006-018933) and Portuguese Fundação para a Ciência e Tecnologia (PTDC/EQU-EQU/71645/2006 and SFRH/BD/31257/2006).

Appendix A. Influence of mass transport on measured binding rate constants

Fig. A.1 shows a schematic of the Biacore's flow chamber. We assume that laminar flow is fully developed over the entire length l of the flow cell and neglect any variations along the z coordinate. Under these assumptions, the velocity field (u, v), which is the solution for fully developed laminar flow between two parallel flat plates, is

$$u = 6\,\bar{u}\left(\frac{y}{h}\right)\left(1-\frac{y}{h}\right), \quad v = 0, \tag{50}$$

where u and v are the velocity components along the x and y coordinates, respectively, and $\bar{u}$ is the average velocity; $\bar{u}$ is related to the volumetric flow rate Q through $\bar{u} = Q/(hw)$ (see Fig. A.1 for the meaning of w and h). Given that $h \gg d_p$, we can linearize the velocity field near $y = 0$; this gives

$$u(y) \approx \frac{6\bar{u}}{h}y \quad \text{for} \quad y \approx 0. \tag{51}$$

At a flow rate of 100 μL/min = 100 mm^3/min, the average axial velocity of an analyte molecule in the flow cell is $\bar{u} = 66.7$ mm/s; However, the average axial velocity of the analyte molecules within the fluid film delimited in the depth $y \leq d_p$ of the evanescent electomagnetic field is reduced to $\bar{u}' = 0.6$ mm/s. Nevertheless, the characteristic residence time of these molecules in the volume of fluid probed the Biacore sensor is only $l_c/\bar{u}' = 1.6/0.6 = 2.8$ seconds (cf. Fig. A.1).

The effect of mass transfer on the analysis of the SPR signal is usually described by a two-compartment model [18]:

$$d_p\frac{dc_B}{dt} + \left(\frac{dq_1}{dt} + \frac{dq_2}{dt}\right) = k_m(c_B^o - c_B), \tag{52}$$

where k_m is the transport coefficient describing the diffusional flux of solute from the bulk of the flow chamber, where its concentration is c_B^o, into the inner compartment, where its concentration is c_B. As a matter of convenience, the inner compartment can be taken as the layer of fluid delimited in the depth of the evanescent electromagnetic field, whose volume is $l_c w_c d_p$ (cf. Fig. A.1).

As discussed by Lok et al. [28] and Sjölander and Urbaniczky [29], it can be shown that, to a good approximation,

$$k_m \approx 1.282\left(\frac{\bar{u}'D^2}{d_p l_c}\right)^{1/3}, \tag{53}$$

where D is the molecular diffusion coefficient.

Transport effects will not influence the adsorption kinetics if $k_m \gg k_r q_1^\infty$ and $k_m \gg k_a q_2^\infty$; similarly, the desorption kinetics will not be influenced by mass transfer if $k_m c_B^o \gg k_d q_2^\infty$. For our SPR experiments with BSA, $D = 9 \times 10^{-7}$ cm^2/s and $k_m = 0.0035$ cm/s. From the data listed in Table 2, it is clear that mass transport effects can be safely neglected in the analysis of the SPR experiments carried out during this work.

References

[1] A. Davies, A. Greene, E. Lullau, W.M. Abbott, Protein Expr. Purif. 42 (2005) 111.
[2] L.W. Pampel, R. Boushaba, N.J. Titchener-Hooker, Biotechnol. Prog. 24 (2008) 192.
[3] J.L. Coffman, J.F. Kramarczyk, B.D. Kelley, Biotechnol. Bioeng. 100 (2008) 605.
[4] K. Rege, M. Pepsin, B. Falcon, L. Steele, M. Heng, Biotechnol. Bioeng. 93 (2006) 618.
[5] D.L. Wensel, B.D. Kelley, J.L. Coffman, Biotechnol. Bioeng. 100 (2008) 839.
[6] T. Vicente, M.F.Q. Sousa, C. Peixoto, J.P.B. Mota, P.M. Alves, M.J.T. Carrondo, J. Membr. Sci. 311 (2008) 270.
[7] T. Rodrigues, A. Carvalho, A. Roldao, M.J.T. Carrondo, P.M. Alves, P.E. Cruz, J. Chromatogr. B 837 (2006) 59.
[8] R. Specht, B. Han, S.R. Wickramasinghe, J.O. Carlson, P. Czermak, A. Wolf, O.W. Reif, Biotechnol. Bioeng. 88 (2004) 465.
[9] K. Yamada, D.M. McCarty, V.J. Madden, C.E. Walsh, Biotechniques 34 (2003) 1074.
[10] A.L. Zydney, C. Harinarayn, R.v. Reis, Biotechnol. Bioeng. 102 (2008) 1131.
[11] E.I. Trilisky, A.M. Lenhoff, J. Chromatogr. A 1142 (2007) 2.
[12] N. Kaludov, B. Handelman, J.A. Chiorini, Hum. Gene Ther. 13 (2002) 1235.
[13] T. Vicente, C. Peixoto, M.J.T. Carrondo, P.M. Alves, Gene Ther. 16 (2009) 766.
[14] B.D. Kelley, M. Switzer, P. Bastek, J.F. Kramarczyk, K. Molnar, T. Yu, J.L. Coffman, Biotechnol. Bioeng. 100 (2008) 950.
[15] X.D. Hoa, A.G. Kirk, M. Tabrizian, Biosens. Bioelectron. 23 (2007) 151.
[16] P. Pattnaik, Appl. Biochem. Biotechnol. 126 (2005) 79.
[17] R.L. Rich, D.G. Myszka, J. Mol. Recognit. 21 (2008) 355.
[18] D.G. Myszka, X. He, M. Dembo, T.A. Morton, B. Goldstein, Biophys. J. 75 (1998) 583.
[19] L.S. Jung, C.T. Campbell, T.M. Chinowsky, M.N. Mar, S.S. Yee, Langmuir 14 (1998) 5636.
[20] M. Mrksich, G.M. Whitesides, Annu. Rev. Biophys. Biomol. Struct. 25 (1996) 55.
[21] G.M. Whitesides, J.K. Kriebel, J.C. Love, Sci. Prog. 2005 (2005) 17.
[22] D.K. Roper, S. Nakra, Anal. Biochem. 348 (2006) 75.
[23] H.S. Kim, S.H. Jung, S.H. Kim, I.B. Suh, W.J. Kim, J.W. Jung, J.S. Yuk, Y.M. Kim, K.S. Ha, Proteomics 6 (2006) 6426.
[24] W. Knoll, F.-J. Schmitt, C. Klein, H.-J. Guder, M. Liley, J. Spinke, US Patent 5,763,191 (1998).
[25] C.A. Brooks, S.M. Cramer, AIChE J. 38 (1992) 1969.
[26] J.C. Bosma, J.A. Wesselingh, AIChE J. 44 (1998) 2399.
[27] PSE, Process systems enterprise, gproms, www.psenterprise.com/gproms, 1997–2009, 2009.
[28] B.K. Lok, Y.-L. Cheng, C.R. Robertson, J. Colloid Interf. Sci. 91 (1983) 104.
[29] S. Sjölander, C. Urbaniczky, Anal. Chem. 63 (1991) 2338.